Langmuir

ARTICLE

pubs.acs.org/Langmuir

# Self-Complementary Recognition of Supramolecular Urea−Aminotriazines in Solution and on Surfaces

Anika Embrechts,[†,‡] Aldrik H. Velders,[§] Holger Schönherr,[*,‡,∥] and G. Julius Vancso[*,‡]

[‡]Department of Materials Science and Technology of Polymers, MESA[+] Institute for Nanotechnology, University of Twente, Post Office Box 217, 7500 AE Enschede, The Netherlands

[§]BioMedicalChemistry, MIRA Institute for Biomedical Technology and Technical Medicine, University of Twente, Post Office Box 217, 7500 AE Enschede, The Netherlands

[∥]Department of Physical Chemistry I, University of Siegen, Adolf-Reichwein-Straße 2, 57076 Siegen, Germany

Supporting Information

**ABSTRACT:** The recognition of self-complementary quadruple urea−aminotriazine (UAT)-based hydrogen-bonded arrays was investigated in solution and at surfaces. For this purpose, an UAT-based donor−acceptor−donor−acceptor (DADA) array and complementary receptors were synthesized. Two-dimensional proton nuclear magnetic resonance ($^1$H NMR) measurements in $CDCl_3$ pointed at an intramolecular hydrogen-bond stabilization of the UAT, which promotes a planar molecular geometry and, thereby, results in a significant stabilization of the dimeric complex. The bond strength of the UAT dimers at surfaces was determined by atomic force microscopy-based single molecule force spectroscopy (AFM−SMFS) in hexadecane. The UAT receptor was immobilized on gold surfaces using an ultrathin layer of ethylene glycol terminated lipoic acid and isocyanate chemistry. The layers obtained and the reversible self-complementary recognition were thoroughly characterized with contact angle measurements, grazing angle Fourier transform infrared (FTIR) spectroscopy, X-ray photoelectron spectroscopy (XPS), and AFM. Loading rate-dependent SMFS measurements yielded a barrier width $x_\beta$ and a bond lifetime at zero force $t_{off}(0)$ of 0.29 ± 0.02 nm and 100 ± 80 ms, respectively. The value of the corresponding off-rate constant $k_{off}$ suggests a substantially larger value of the dimerization constant compared to theoretical predictions, which is fully in line with the additional intramolecular hydrogen-bond stabilization detected in solution by $^1$H NMR spectroscopy.

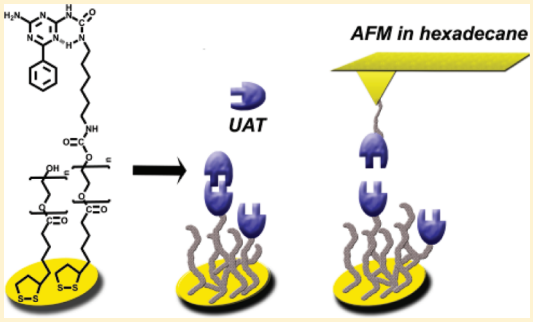


## INTRODUCTION

Supramolecular materials are known for their special properties, including self-healing.[1] As was demonstrated by Sijbesma, Meijer, and co-workers[2] and more recently by Leibler and co-workers,[3] a new and exciting class of polymer materials can be ingeniously designed using supramolecular hydrogen-bonding building blocks, such as, for instance, widely available urea moieties. The properties of these hydrogen-bonded polymers strongly depend upon the number and strength of the hydrogen-bonded arrays that form the reversible interaction between polymer segments. To be able to understand structure−property relationships and design these materials, it is of vital importance to identify the key molecular contributors to hydrogen-bond strength in solution. Previous studies by Sijbesma and Meijer[4,5] already indicated that these contributions are insufficiently covered by currently available models,[6] which are based on primary and secondary hydrogen-bond interactions. For an enhanced understanding and control, additional experimental data are needed, which at the same time provide further insight into the bulk properties of these systems.

The (hydrogen-)bond strength of complexes in different solvents is usually determined using the concentration-dependent transition of dimers to monomers in the solvent of interest, which is determined by isothermal titration calorimetry (ITC) or nuclear magnetic resonance (NMR) spectroscopy. The analysis of arrays with high dimerization constants in (relatively) nonpolar solvents, such as chloroform, requires more sensitive techniques, e.g., fluorescence spectroscopy.[5]

On a single molecule scale, force measurements provide complementary insight into the energy landscape of complex unbinding. Using atomic force microscopy based single molecule force spectroscopy (AFM−SMFS),[7] bond strengths are probed for different bond loading rate (stretching rate) conditions for single molecules.[8] Using this technique, a comparison of the hydrogen-bond strength of complementary quadruple hydrogen-bonded arrays in a highly apolar solvent (hexadecane) becomes feasible because of the loading rate-dependent energy

**Received:** September 1, 2011
**Revised:** September 30, 2011
**Published:** October 04, 2011

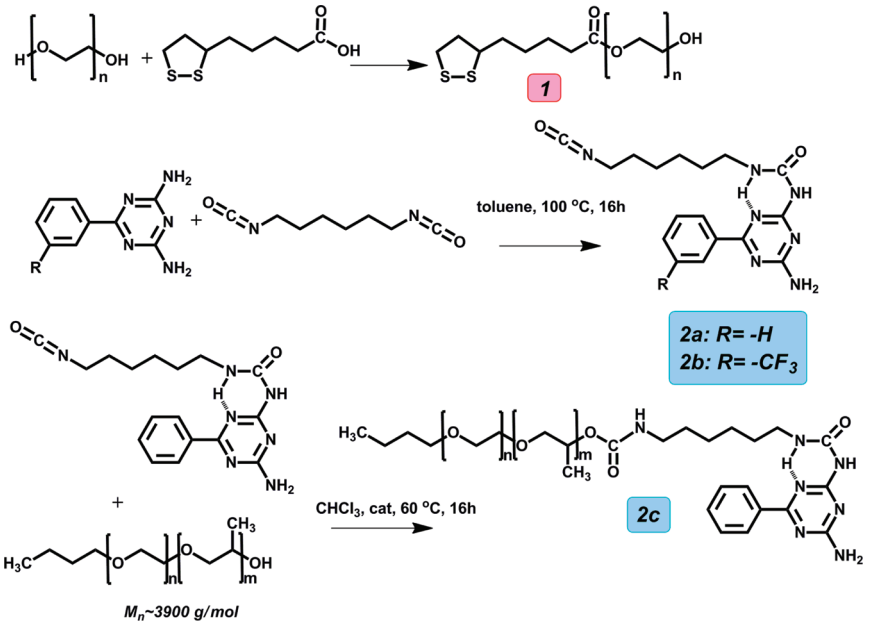


**Figure 1.** Synthesis of a PEG-terminated lipoic acid (**1**) and UAT-based hydrogen-bond moieties (**2a**−**2c**) with a DADA recognition site for complementary hydrogen-bond formation and different side-group functionalization.

landscape of the bond.[8,9] Solubility issues are circumvented, because AFM-based SMFS experiments can be performed at low concentrations (from micromolars to nanomolars). In the framework of the Evans−Bell formalism,[8] these measurements provide direct estimates of the barrier width $x_\beta$ and the bond lifetime at zero force $t_{off}(0)$. In addition, these experiments provide an opportunity to identify the influence of the immediate surrounding on the bond strength of the ligand−receptor interaction. AFM-based SMFS was previously used by us to study the binding strength[9] and supramolecular polymer formation[10] of the well-known ureidopyrimidinone [UPy, donor−donor−acceptor−acceptor (DDAA)] array in hexadecane.[9] Single molecule and bulk studies on supramolecular polymer formation of ureidopyrimidinones were also performed by Guan and coworkers.[11]

To obtain more detailed insight into the key contributions that determine the hydrogen-bond strength in designed synthetic systems, e.g., the influence of molecular structure and geometry, we studied a newly synthesized urea−aminotriazine (UAT)-based hydrogen-bonded array with donor−acceptor−donor−acceptor (DADA) arrangement (Figure 1) and compared the experimentally accessible off rates to predictions from theory. The single molecule data acquired by AFM−SMFS were complemented by two-dimensional (2D) $^1$H NMR results acquired in solution.

## EXPERIMENTAL SECTION

**Preparation of Substrates.** Gold substrates (200 nm gold on top of 3.5 nm Ti deposited onto glass substrates) were purchased from Ssens BV (Hengelo, The Netherlands). Prior to use, these substrates were cleaned in Piranha solution [2:1 $H_2SO_4$ (Sigma-Aldrich)/$H_2O_2$ (30%, Fluka) by volume], then rinsed 3 times with Milli-Q water and ethanol, and subsequently, rinsed with the pure solvent. The samples were directly transferred to the monolayer solution preventing any direct contact with air. Caution: Piranha solution should be handled with extreme caution. It has been reported to detonate unexpectedly.

**Preparation and Characterization of Monolayers.** Monolayers were prepared by immersing (annealed) gold substrates into a dilute solution of the corresponding compound for at least 16 h (typical concentration of 1 mM). Figure 3 shows the reaction scheme for the preparation of the different layers. After rinsing in dichloromethane or chloroform and drying in a nitrogen stream, the measurements were performed with minimum delay. The layers were characterized by contact angle measurements, X-ray photoelectron spectroscopy (XPS), Fourier transform infrared (FTIR) spectroscopy, and AFM.

**General Characterization Methods.** The $^1$H NMR spectra were recorded on a Varian Unity 300, in $CDCl_3$, and chemical shifts are given relative to the residual $CHCl_3$ peak (7.26 ppm). Two-dimensional $^1$H NMR experiments and $^1$H NMR on polymers (see the Supporting Information) were performed on a Bruker 600 MHz Avance II NMR spectrometer. Electron spray ionization mass spectrometry was performed on a Waters LCT. FTIR bulk measurements were performed on a Bruker Alpha-P.

**XPS.** XPS spectra were recorded using a PHI Quantera scanning XPS microprobe (SXM) from Physical Electronics. Spectra were acquired using a monochromated X-ray beam (Al K$\alpha$, monochromatic at 1486.6 eV) with the following beam specifications: 100 $\mu$m diameter, 25 W, and 45° takeoff angle. Atomic concentrations were determined by numerical integration of the relative peak areas in the detailed element scans using the following sensitivity factors: Au(4f), 6.805; C(1s), 0.314; N(1s), 0.499; O(1s), 0.733; and S(2p), 0.717.

**AFM Measurements.** The measurements were carried out with a Veeco/Bruker Multimode with a NanoScope V controller (Veeco/Bruker, Santa Barbara, CA). The calibration of the AFM scanner in the $z$ direction was carried out using a set of three vertical calibration standards (TGZ 01−03), with step heights of 25.5, 104, and 512 nm, respectively (Silicon-MDT, Moscow, Russia). A double-sided gold-coated MikroMasch rectangular beam cantilever (CSC38) was used (the spring constant was determined by the thermal noise method[12] to be $k = 0.133 \pm 0.014$ N/m).

## RESULTS AND DISCUSSION

The synthesis of substituted UAT derivatives is shown in Figure 1. On the basis of previously established chemistry for

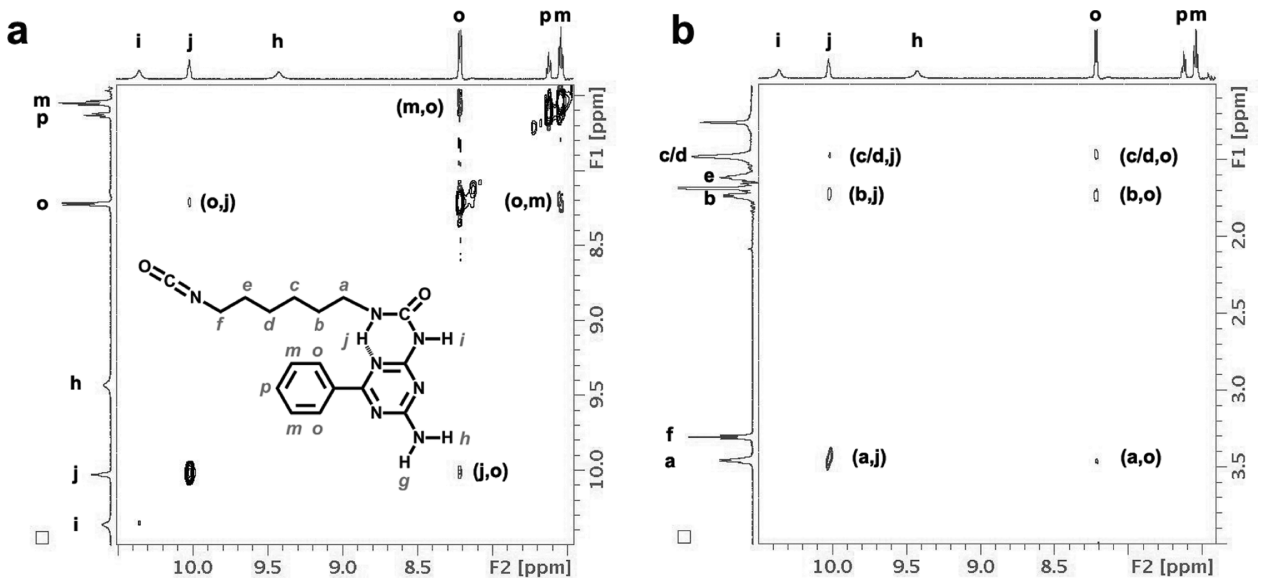


**Figure 2.** Two-dimensional $^1$H NMR spectrum of UAT recorded in deuterated chloroform using rotating-frame Overhauser effect spectroscopy (ROESY) at 265 K. (a) At low field, NOEs between adjacent nuclei can be observed for the urea hydrogen involved in the intramolecular hydrogen bond, (j) at 10.0 ppm, with the *ortho* hydrogens of the phenyl group, (o) at 8.2 ppm. (b) At high field, the (j) urea and (o) *ortho* protons show NOEs with the aliphatic $CH_2$ groups (b−d) at 1.7−1.3 ppm. (Inset) Derived spatial arrangement of the self-complementary hydrogen-bonded array in solution.

UPy synthesis,[13] the poly(ethylene glycol) (PEG)-terminated lipoic acid[14] (**1**) and the UAT-based quadruple hydrogen-bonded array (**2a**) were synthesized. Compound **2a** was synthesized following a slightly adapted procedure described previously by Sijbesma and Meijer.[2] Complementary UAT receptors comprising trifluoromethyl (**2b**) and PEG−poly(propylene oxide) (PPO) (**2c**) substituents were synthesized using the same isocyanate chemistry.

The UAT-based compounds were characterized using mass spectrometry, FTIR, and $^1$H NMR [one-dimensional (1D) and 2D] spectroscopy. In particular, variable-temperature and 2D $^1$H NMR experiments provided additional information for the correct assignment of the hydrogen-bond interactions. $^1$H NMR spectra of a saturated UAT solution were recorded in deuterated chloroform at two different temperatures (295 and 265 K), and the signals were assigned using correlation spectroscopy (COSY; see the Supporting Information) and nuclear Overhauser effect (NOE) data. The 1D $^1$H spectrum of UAT shows the characteristic pattern for hydrogen-bonded dimers, with the two protons involved in the quadruple hydrogen bonds being significantly shifted downfield (see 9.3 and 10.3 ppm for i and h, respectively, in Figure 2). The amine proton not involved in the hydrogen-bonding resonates at 5.5 ppm. Interestingly, the urea proton is observed at very low field (10.0 ppm); the corresponding signal is relatively sharp and does not change when the temperature is decreased. This indicates that this proton is involved in intramolecular hydrogen bonding with the neighboring triazine nitrogen.

Because of the dynamic behavior of the aliphatic chain and the fast rotation of the phenyl ring on the NMR time scale, as concluded from the single set of *ortho* and *meta* proton signals, NOE cross-peaks are only weak at room temperature. Lowering the temperature, however, allows for the recording of a rotating-frame Overhauser effect spectroscopy (ROESY) spectrum with cross-peaks that further corroborate the intramolecular hydrogen bond of the urea proton with the triazine. The ROESY spectrum shown in Figure 2 displays characteristic NOE cross-peaks for the *ortho* protons of the phenyl ring with the urea proton (Figure 2a) and with the methylene protons of the aliphatic chain (Figure 2b), respectively. The intramolecular hydrogen bond is apparently strongly orienting the aliphatic chain, which, therefore, lies parallel to the triazine−phenyl ring system, explaining the NOE cross-peaks. Interestingly, the NOE cross-peak of the phenyl−*ortho* protons with the methylene "b" and "c/d" protons and urea−NH are stronger than the NOE cross-peak with the methylene "a" protons. This further confirms the strong intramolecular hydrogen bond and orientation of the aliphatic chain.

For the single molecule experiments, a layer of compound **1** was prepared on gold,[9,13] which was end-functionalized with the UAT-based hydrogen-bonded moiety **2a** (Figure 3).

The established procedure results in a low surface coverage of the UAT moieties, which is a prerequisite for single molecule detection by AFM−SMFS. The layers on gold were characterized by contact angle measurements, grazing angle FTIR spectroscopy, XPS, and AFM. The initial layer of compound **1** showed advancing and receding contact angles of 38° ± 2° and 23° ± 1°, respectively, while the UAT functionalized layers (**1** + **2a**) displayed advancing and receding contact angles of 61° ± 4° and 24° ± 2° for low surface coverage of the UAT moiety and 76° ± 3° and 56° ± 3° for higher surface coverage. This substantial increase in the contact angle is attributed to the phenyl rings that now reside at the surface.[15] When this layer was immersed in the complementary solution of PEGPPO−UAT (**2c**) (in $CHCl_3$) and rinsed afterward, advancing and receding contact angles of 56° ± 2° and 24° ± 2° were measured. After the sample was thoroughly rinsed with dimethylsulfoxide (DMSO), the advancing and receding contact angles were determined to be 71° ± 3° and 49° ± 2°, respectively. These contact angle data show that the complexation is reversible, because the contact angle of the PEG−UAT layers is almost completely recovered

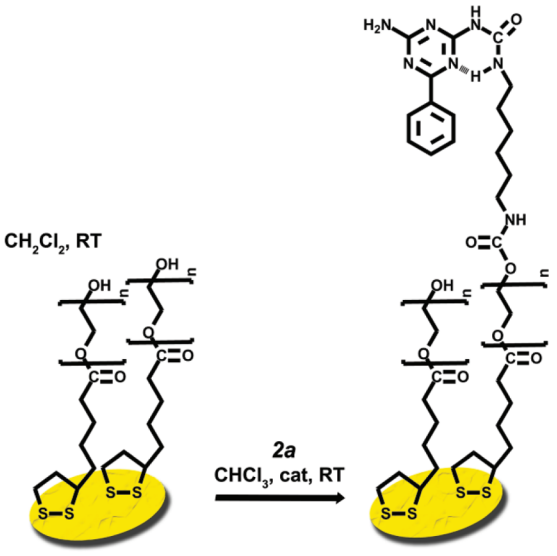


**Figure 3.** Schematic of the immobilization of UAT moieties on gold. A layer of PEG with exposed terminal hydroxy groups (**1**) is formed by adsorption from solution on gold, followed by the reaction with compound **2a** to afford UAT end-functionalized PEG chains.

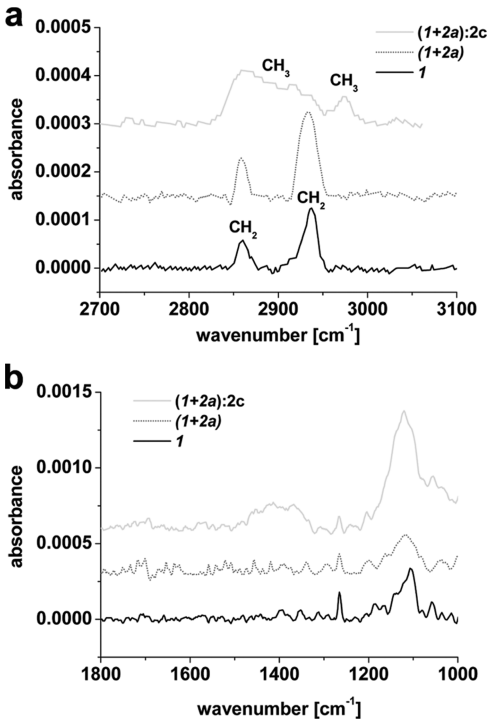


**Figure 4.** (a and b) Grazing incidence reflection FTIR spectra captured on gold of (bottom) PEG (**1**), (middle) PEG−UAT (**1** + **2a**), and (top) compounds **1** + **2a** after the interaction with the complementary PEGPPO−UAT (**2c**), respectively. In the spectral region around 3000 $cm^{-1}$, the $CH_3$ groups of the PPO are clearly detectable after the reaction of compounds **1** + **2a** with compound **2c**. The C−O−C stretching vibrations of the PEG moieties are observed at wavenumbers of approximately 1100 $cm^{-1}$. The broad peaks at 1114 and 1130 $cm^{-1}$ indicate disordered PEG, i.e., PEG in a noncrystalline environment.

after functionalization and subsequent rinsing with DMSO, which is known to break hydrogen bonds.[16]

FTIR measurements in bulk and on the functionalized layer were performed to characterize the different layers as well (Figure 4). PEG layer of compound **1** on gold shows distinct but slightly shifted $CH_2$ stretching vibrations (in comparison to a self-assembled monolayer of octadecanethiol), which can be attributed to a randomly coiled PEG layer with additional $CH_2$ stretches from the lipoic acid ring.[17] Because a submonolayer is obtained using this technique, PEG may adopt very different conformations on the surface, which leads to peak broadening in the FTIR spectrum. This is also apparent for the C−O−C stretches, which broaden from a sharp peak at 1002 $cm^{-1}$ (crystalline bulk) to a broad peak from 1002 to 1143 $cm^{-1}$. Although there is a small increase in the $CH_2$ intensity and small additional peaks from 1400 to 1600 $cm^{-1}$ ($CH_2$, urethane, phenyl, and triazine stretches), the addition of UAT moieties on top of the PEG layer can only barely be detected.

As observed from Figure 4, submersion of the UAT end-functionalized layer (**1** + **2a**) in a complementary PEGPPO−UAT solution (**2c**) and subsequent rinsing introduces $CH_3$ vibrations in the spectrum, as well as a clear increase of the C−O−C stretches around 1100 and 1325−1500 $cm^{-1}$ (mostly additional $CH_2$ and $CH_3$ stretches). In addition, peak broadening around 1100 $cm^{-1}$ can also be observed because of PPO. The integral increases of the $CH_2$−$CH_3$ region and the C−O−C region are both consistent with the interaction of the PEGPPO tail.

XPS analysis[18] of the layers of compound **1** and PEG−UAT (**1** + **2a**) provided evidence for the selective adsorption of the PEG molecules to the gold surface, because the S(2p) binding energy was shifted to lower values (90% S−Au) compared to free sulfur bonds.

Furthermore, the C(1s) spectra in Figure 5 displays a distinct C−O−C peak from the PEG layer (286.8 eV) for both samples. However, some additional aliphatic carbon is detected, which can be attributed to an adventitious carbon layer for PEG substrates with low surface coverage.[18] Using a correction for the added adventitious carbon, a surface coverage of the hydrogen-bonded moieties of 11 ± 6% could be determined from the ratios of the atomic percentages of nitrogen with respect to sulfur determined from the corresponding N(1s) [binding energy (BE) = 400.5 eV] and S(2p) (BE = 162.5 eV) peaks[18] (see the Supporting Information).

The forced unbinding of UAT dimers was subsequently studied in AFM-based SMFS experiments, which is schematically shown in Figure 6.

Recognition AFM experiments[19] were performed in hexadecane at different loading rates (Figure 7). The rupture force of each single molecule rupture event was determined using the PEG linker as a molecular extension length marker for single molecule probing. This approach enabled us to determine various important parameters of the potential-energy landscape along the unbinding axis, as was initially demonstrated by Bell.[8] The single molecule rupture events were studied at different loading rates covering 2 orders of magnitude. For each loading rate, the most probable rupture force $f^*$ was determined using Gaussian fitting.[20] Dimer rupture was identified by considering only data with stretch lengths between 10 and 25 nm (estimated on the polydispersity of the PEG linker and the attached UAT moiety). According to Ray et al., the polydispersity of the PEG linker leads to an

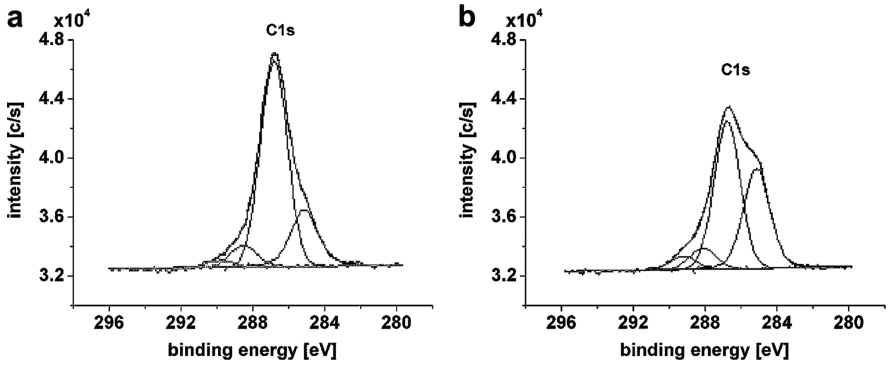


**Figure 5.** (a and b) C(1s) XPS spectra for the C1s peak for layers of PEG (**1**) and PEG−UAT (**1** + **2a**). The abundance of different carbon bonds (aliphatic, C−O, and C═O) was determined via deconvolution using the relative energy shifts of the respective bonds. The C−O−C peaks from the PEG layer located at 286.8 eV can be clearly discerned in both samples. Note that the amount of aliphatic and aromatic carbon (285.0 eV) increases from a to b because of the reaction with the hydrogen-bonded moiety **2a** in combination with adventitious carbon deposition.[18]

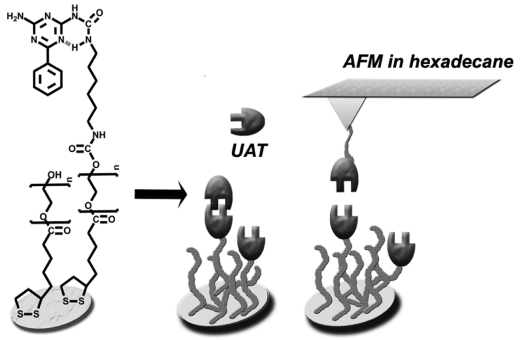


**Figure 6.** Schematic of the modified gold surface.

estimated error of 2% in $f^*$.[21] The stretching of individual PEG chains was further confirmed by successfully fitting the force extension curves to the wormlike chain (WLC), which yielded loading-rate-independent mean values for the persistence length ($l_p$) of 3.35 ± 0.49 Å, which agrees well with the literature data. According to the literature, the helical state monomer length of PEG is 2.78 Å and a $l_p$ = 3.81 ± 0.02 Å (WLC) and Kuhn length $l_K$ = 7 Å [from a fit to the freely joined chain (FJC) model] were previously reported.[22] In our measurements, the difference between the elasticity parameters obtained from fits to the WLC and FJC models is negligible, because small extensions at low rupture forces were studied. In that case, the following expression for the relation of the persistence length and Kuhn length applies: $l_p = 1/2l_K$. Hence, the average $l_p$ of 3.35 ± 0.49 Å is in line with previously reported data and confirms that indeed single chains were stretched and, hence, single molecule rupture events were probed.

The Bell−Evans approach of loading-rate-dependent bond rupture analysis[8] was applied to obtain a value for the thermal scale force $f_\beta$ by fitting the measured data to eq 1 via a Marquardt−Levenberg algorithm (Figure 7d). This approach is based on the fact that measurements are performed far from equilibrium conditions, where the chance of rebinding between receptor and ligand approaches zero, because of the flexible polymer linker. In this case, the most probable rupture force of dissociation logarithmically depends upon the applied loading rate. Therefore, the kinetic off-time can be directly determined via these experiments.

According to the Bell−Evans theory, the thermal scale force $f_\beta$ correlates the most probable rupture force $f^*$ with the loading rate $r_f$, as displayed in eq 1.

$$f^* = f_\beta \ln\left(\frac{r_f}{r_f^0}\right) \quad (1)$$

The Bell−Evans approach provided the following parameters: $f_\beta$ = 14.5 ± 1.1 pN and $r_f^0 = (1.5 \pm 0.9) \times 10^2$ pN/s. Using the fitted value of $f_\beta$ and the intercept at zero force $r_f^0$, the bond lifetime for the mechanical stress-free state $t_{off}$ ($f$ = 0) can be determined.

$$t_{off}(0) = \frac{f_\beta}{r_f^0} \quad (2)$$

On the basis of these parameters, the barrier width $x_\beta$ and the bond lifetime at zero force can be determined as well: $x_\beta$ = 0.29 ± 0.02 nm[23] and $t_{off}(0)$ = 100 ± 80 ms.

From the dimerization constant predicted from the currently available models for UAT in hexadecane ($K_{dim} = 3 \times 10^4$ $M^{-1}$) and assuming diffusion-limited association for the reaction in solution with $k_{on} = 10^8$ $M^{-1}$ $s^{-1}$, a $k_{off} = 3.3 \times 10^3$ $s^{-1}$ and, correspondingly, a bond lifetime $t_{off} \approx 0.3$ ms can be estimated.[24] This value is 3 orders of magnitude smaller than the value observed in the SMFS experiments.

The marked discrepancy shows that the complex is much more stable than predicted on the basis of the simple model. A correspondingly inferred higher binding constant can be tentatively attributed to the influence of the intramolecular hydrogen bond, which promotes a planar molecular geometry and significantly stabilizes the dimeric complex, as confirmed using 2D $^1$H NMR (compare to Figure 2). Because these models are only based on primary and secondary hydrogen-bond interactions, the effect of the planarized molecular geometry is not covered. Recent literature also demonstrated the importance of geometric configuration[25] and substituents,[26] in which a wide range of dimer equilibrium constants in chloroform could be obtained by fine-tuning the substituent attached to the same DDAA or DADA quadruple hydrogen-bonded array. Most notably is the dramatic 800-fold decrease of the dimer equilibrium constant of a UPy (DDAA) hydrogen-bonded array because of a directly attached oligomeric ethylene glycol chain,[26] which provides evidence for the major influence of substituents as (de)stabilizing factors on the dimer bond strength. The data obtained here is,

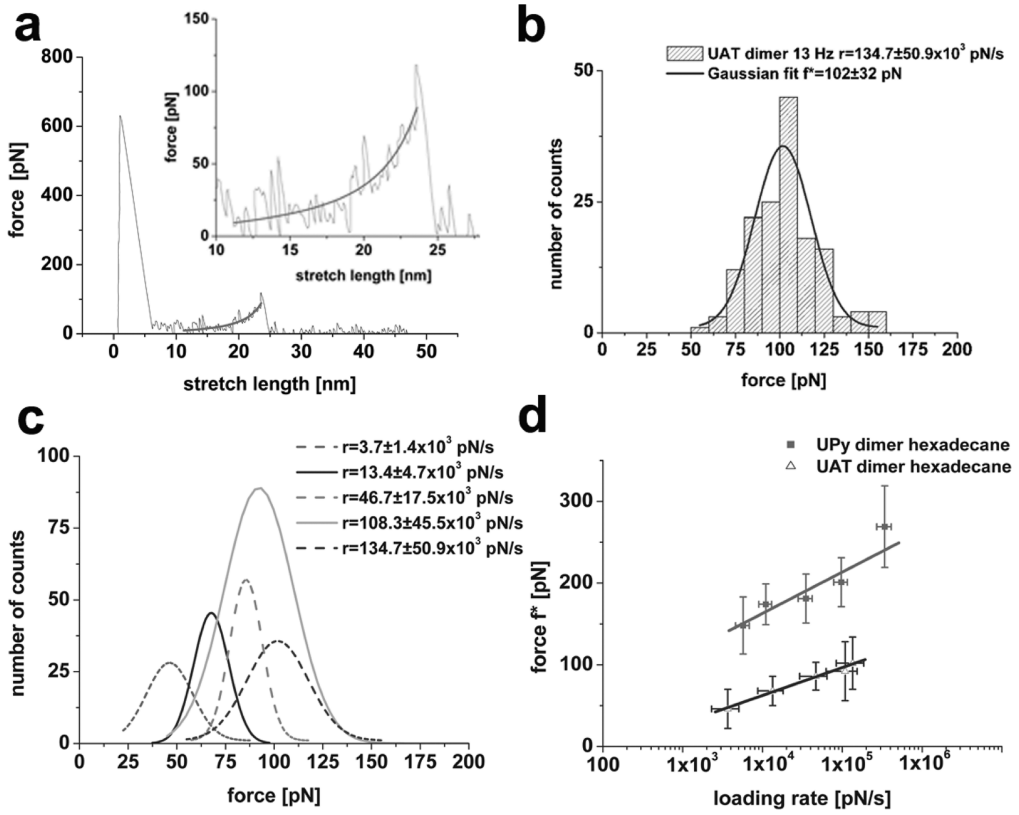


**Figure 7.** SMFS data and analysis of UAT dimer bond rupture for different loading rates in hexadecane. (a) Force extension curve showing a single molecule rupture event of UAT dimer at a loading rate of $r_f = (134.7 \pm 50.9) \times 10^3$ pN/s. (b) Histogram of bond rupture forces of UAT dimers, with most probable rupture force $f^* = 102 \pm 32$ pN and loading rate $r_f = (134.7 \pm 50.9) \times 10^3$ pN/s. (c) Overview of Gaussian fits of histograms of UAT dimer bond rupture for different loading rates [$r_f = (3.7-134.7) \times 10^3$ pN/s] in hexadecane. (d) Loading rate dependence of UAT dimers [$T = 303 \pm 2$ K; $f_\beta = 14.5 \pm 1.1$ pN; and $t_{off}(0) = 100 \pm 80$ ms] compared to UPy dimers [$T = 303 \pm 2$ K; $f_\beta = 21.3 \pm 2.0$ pN; and $t_{off}(0) = 3.9 \pm 0.9$ s].

hence, qualitatively in line with the measured binding constants for similar DADA arrays measured in chloroform by Sijbesma and Meijer[4] by NMR binding studies ($K_{dim} = 2 \times 10^4 - 2 \times 10^5$ $M^{-1}$), which would lead to extrapolated values of $K_{dim} \sim 2 \times 10^6 - 2 \times 10^7$ $M^{-1}$ in hexadecane.

## CONCLUSION

A UAT-based DADA array was synthesized, and the dimeric complex was investigated in solution and on gold surfaces. Variable-temperature 1D and 2D $^1$H NMR results acquired in chloroform indicated an additional intramolecular hydrogen-bond stabilization, which promotes a planar molecular geometry and significantly stabilizes the dimeric complex. These continuum data are corroborated by AFM−SMFS data obtained in hexadecane. The bond lifetime in the absence of force extrapolated from the loading rate dependence of the most probable rupture forces exceeds the bond lifetime estimated from the additive primary and secondary hydrogen-bonding interactions by 3 orders of magnitude.

## ASSOCIATED CONTENT

**Supporting Information.** Synthesis and analysis results (1D and 2D $^1$H NMR, electron spray mass spectrometry, and FTIR) of the synthesized materials, XPS results on gold surfaces, and AFM−SMFS measurements. This material is available free of charge via the Internet at http://pubs.acs.org.

## AUTHOR INFORMATION

### Corresponding Author

*Fax: (+49) 271-740-2805 (H.S.); (+31) 53-489-3823 (G.J.V.). E-mail: schoenherr@chemie.uni-siegen.de (H.S.); g.j.vancso@utwente.nl (G.J.V.).

### Present Addresses

[†]Department of Chemical Engineering, Section Nanostructured Materials, Delft University of Technology, Julianalaan 136, 2628 BL Delft, The Netherlands.

## ACKNOWLEDGMENT

We thank Prof. Dario Anselmetti, Prof. Peter Hinterdorfer, and Mr. Gerard Kip for fruitful discussions. This work has been financially supported by the Council for Chemical Sciences of The Netherlands Organization for Scientific Research (CW-NWO), ECHO Grant 754021 and NWO Middelgroot Grant 700.54.102.

## REFERENCES

(1) Bergman, S. D.; Wudl, F. *J. Mater. Chem.* **2008**, *18*, 41–62.
(2) Folmer, B. J. B.; Sijbesma, R. P.; Versteegen, R. M.; van der Rijt, J. A. J.; Meijer, E. W. *Adv. Mater.* **2000**, *12*, 874–878.
(3) Montarnal, D.; Tournilhac, F.; Hidalgo, M.; Couturier, J.-L.; Leibler, L. *J. Am. Chem. Soc.* **2009**, *131*, 7966–7968.

(4) Beijer, F. H.; Kooijman, H.; Spek, A. L.; Sijbesma, R. P.; Meijer, E. W. *Angew. Chem., Int. Ed.* **1998**, *37*, 75–78.
(5) (a) Beijer, F. H.; Sijbesma, R. P.; Kooijman, H.; Spek, A. L.; Meijer, E. W. *J. Am. Chem. Soc.* **1998**, *120*, 6761–6769. (b) Söntjens, S. H. M.; Sijbesma, R. P.; van Genderen, M. H. P.; Meijer, E. W. *J. Am. Chem. Soc.* **2000**, *122*, 7487–7493.
(6) Sartorius, J.; Schneider, H.-J. *Chem.—Eur. J.* **1996**, *2*, 1446–1452.
(7) (a) Hugel, T.; Seitz, M. *Macromol. Rapid Commun.* **2001**, *22*, 989–1016.(b) Zhang, X.; Liu, C.; Shi, W. *Physical Properties of Polymers Handbook*; Springer: Berlin, Germany, 2007; pp 525−535.
(8) (a) Bell, G. I. *Science* **1978**, *200*, 618–627. (b) Merkel, R.; Nassoy, P.; Leung, A.; Ritchie, K.; Evans, E. *Nature* **1999**, *397*, 50–53. (c) Evans, E. *Annu. Rev. Biophys. Biomol. Struct.* **2001**, *30*, 105–128.
(9) Zou, S.; Schönherr, H.; Vancso, G. J. *J. Am. Chem. Soc.* **2005**, *127*, 11230–11231.
(10) (a) Zou, S.; Schönherr, H.; Vancso, G. J. *Angew. Chem., Int. Ed.* **2005**, *44*, 956–959. (b) Embrechts, A.; Schönherr, H.; Vancso, G. J. *J. Phys. Chem. B* **2008**, *112*, 7359–7362.
(11) Guan, Z.; Roland, Z. T.; Bai, J. Z.; Ma, S. H.; McIntire, T. M.; Nguyen, M. *J. Am. Chem. Soc.* **2004**, *126*, 2058–2065.
(12) Hutter, J. L.; Bechhöfer, J. *Rev. Sci. Instrum.* **1993**, *64*, 1868–1873.
(13) Zou, S.; Zhang, Z.; Förch, R.; Knoll, W.; Schönherr, H.; Vancso, G. J. *Langmuir* **2003**, *19*, 8618–8621.
(14) Neises, B.; Steglich, W. *Org. Synth.* **1990**, *7*, 93–94.
(15) Kang, J. F.; Liao, S.; Jordan, R.; Ulman, A. *J. Am. Chem. Soc.* **1998**, *120*, 9662–9667.
(16) Hunter, C. A. *Angew. Chem., Int. Ed.* **2004**, *43*, 5310–5324.
(17) (a) Miyazawa, T.; Fukushima, K.; Ideguchi, Y. *J. Chem. Phys.* **1962**, *37*, 2764–2776. (b) Valiokas, R.; Svedhem, S.; Svensson, S. C. T.; Liedberg, B. *Langmuir* **1999**, *15*, 3390–3394. (c) Naumann, R.; Schiller, S. M.; Giess, F.; Grohe, B.; Hartman, K. B.; Kärcher, I.; Lübben, J.; Vasilev, V.; Knoll, W. *Langmuir* **2003**, *19*, 5435–5443. (d) Vanderah, D. J.; Pham, C. P.; Springer, S. K.; Silin, V.; Meuse, C. W. *Langmuir* **2000**, *16*, 6527–6532. (e) Kim, C.-H.; Kim, D.-W.; Cho, K. Y. *Polym. Bull.* **2009**, *63*, 91–99. (f) Buchbinder, A. M.; Weitz, E.; Geiger, F. M *J. Phys. Chem. C* **2010**, *114*, 554–566.
(18) (a) Sharma, S.; Johnson, R. W.; Desai, T. A. *Biosens. Bioelectron.* **2004**, *20*, 227–239.(b) Moulder, J. F.; Stickle, W. F.; Sobol, P. E.; Bomben, K. D. *Handbook of X-ray Photoelectron Spectroscopy*; Perkin-Elmer Corporation: Waltham, MA, 1992. (c) Beamson, G.; Briggs, D. *High Resolution XPS of Organic Polymers: The Scienta ESCA300 Database*; John Wiley and Sons: New York, 1992.
(19) Raible, M.; Evstigneev, M.; Bartels, F. W.; Eckel, R.; Nguyen-Duong, M.; Merkel, R.; Ros, R.; Anselmetti, D.; Reimann, P. *Biophys. J.* **2006**, *90*, 3851–3864.
(20) High loading rates and a flexible polymer linker are used in these experiments. Furthermore, the loading rate is determined as the slope of the force versus time trace close to the actual rupture event. Therefore, Gaussian fitting can directly be applied to determine the most probable rupture force $f^*$ and, subsequently, the thermal scale force $f_\beta$ without the need of, for instance, Monte Carlo simulations, which take into account the linker parameters: $L_b$ (contour length) and $L_p$ (persistence length).
(21) Ray, C.; Brown, J. R.; Akhremitchev, B. B. *J. Phys. Chem. B* **2007**, *111*, 1963–1974.
(22) (a) Oesterhelt, F.; Rief, M.; Gaub, H. E. *New J. Phys.* **1999**, *1*, 6.1–6.11. (b) Kienberger, F.; Pastushenko, V. P.; Kada, G.; Gruber, H. J.; Riener, C.; Schindler, H.; Hinterdorfer, P. *Single Mol.* **2000**, *1*, 123–128.
(23) This characteristic transition-state length $x_\beta = 0.29 \pm 0.02$ nm agrees with the crystallographic data for the intermolecular UAT hydrogen-bond length (0.275−0.325 nm) determined by Sijbesma and Meijer.[4]
(24) On the basis of the theoretical predictions of Sartorius and Schneider[6] ($K$ = 330 $M^{-1}$) for DADA arrays in chloroform and the experimental results of hydrogen-bond strength in a range of apolar solvents by Sijbesma and Meijer,[5b] the hydrogen-bond strength of a DADA array in hexadecane was estimated to be $K = 3 \times 10^4$ $M^{-1}$.
(25) Ligthart, G. B. W. L.; Guo, D.; Spek, A. L.; Kooijman, H.; Zuilhof, H.; Sijbesma, R. P. *J. Org. Chem.* **2008**, *73*, 111–117.
(26) (a) de Greef, T. F. A.; Nieuwenhuizen, M. M. L.; Stals, P. J. M.; Fité, C. F. C.; Palmans, A. R. A.; Sijbesma, R. P.; Meijer, E. W. *Chem. Commun.* **2008**, 4306–4308. (b) de Greef, T. F. A.; Nieuwenhuizen, M. M. L.; Sijbesma, R. P.; Meijer, E. W. *J. Org. Chem.* **2010**, *75*, 598–610.